AIAA JOURNAL
Vol. 57, No. 10, October 2019

Optimization of Supercritical Airfoil Design with Buffet Effect

Zhaoyi Xu,* Joseph H. Saleh,† and Vigor Yang‡
Georgia Institute of Technology, Atlanta, Georgia 30332

DOI: 10.2514/1.J057573

In transonic flight within a certain range of Mach number and angle of attack, the flowfield becomes unstable, and it produces an oscillating aerodynamic force: a phenomenon commonly known as transonic buffet. This load can inflict severe damage on the structure of an aircraft wing, and so it is necessary to consider the buffet effect in supercritical airfoil design. In the present work, the first objective is to find optimal profiles for minimizing the time-averaged drag and buffet magnitude. The second objective is to compare new airfoils and derive insights for transonic supercritical airfoil design to reduce buffet effect. The OAT15A airfoil is chosen as the baseline design, and then a numerical scheme is developed to obtain time-averaged aerodynamic coefficients and buffet parameters. A geometry disturbance method with smoothness check is introduced to develop a set of new airfoils. Simulations of the new airfoils are conducted to populate the sample space for surrogate modeling. A neural network method is used to build the surrogate models, which are then employed in a genetic algorithm to select optimized airfoils. Finally, the behavior and physics of the optimal airfoils are simulated and analyzed.

Nomenclature

A	=	buffet magnitude
a_∞	=	far-field speed of sound
c	=	chord length
c_d	=	drag coefficient
c_{di}	=	drag coefficient at ith step
c_l	=	lift coefficient
c_{li}	=	lift coefficient at ith step
c_p	=	pressure coefficient
$\overline{c_d}$	=	time-averaged drag coefficient
$\overline{c_l}$	=	time-averaged lift coefficient
f	=	buffet frequency
f_A	=	genetic algorithm buffet magnitude optimization object function
f_{c_d}	=	genetic algorithm drag optimization object function
G_k	=	airfoil shape parameter for mode k
g	=	airfoil shape modification basic function
k	=	reduced frequency of buffet
M	=	Mach number
m	=	mean residual
P_c	=	genetic algorithm crossover probability
P_m	=	genetic algorithm mutation probability
p_i	=	genetic algorithm constraint penalty function
R^2	=	coefficient of determination
s	=	airfoil profile
s_A^*	=	magnitude optimal airfoil
$s_{\overline{C_d}}^*$	=	drag optimal airfoil
T	=	computational wall time
V_∞	=	far-field velocity magnitude
α	=	angle of attack
Δt	=	dimensionless time step
δt	=	dimensional time step
ε	=	relative error
ζ_i	=	relaxation coefficient of the constraints in the optimization problem
λ	=	genetic algorithm initial population
σ	=	standard deviation

Received 31 May 2018; revision received 17 September 2018; accepted for publication 25 October 2018; published online 28 December 2018.

*Graduate Student, School of Aerospace Engineering.
†Associate Professor, School of Aerospace Engineering. Associate Fellow AIAA.
‡William R. T. Oakes Professor and Chair, School of Aerospace Engineering; vigor.yang@aerospace.gatech.edu. Fellow AIAA (Corresponding Author).

I. Introduction

IN 1947, Hilton and Fowler [1] detected periodic shock oscillations in their transonic flow experiments for a low drag airfoil. The authors also detected a thickening of the boundary layer downstream behind the shock wave. Although a clear physical understanding of this shock-wave/boundary-layer interaction was not achieved, their result initiated a new research direction into transonic buffet.

In transonic flow with a certain range of attack angle, a shock wave is formed on the airfoil when the Mach number M exceeds a critical value. As the Mach number increases, the shock wave moves toward the trailing edge of the airfoil. A separation zone behind the shock appears and grows in this process. Buffet takes place when the separation zone extends to the trailing edge and interacts with the shock. Figure 1 illustrates the interaction between the shock wave and the boundary layer for the OAT15A airfoil at $M = 0.73$, and $\alpha = 3.5$ deg. The resulting oscillating aerodynamic force acts on the wing structure, and it can degrade aircraft performance. More important, this force fluctuation can severely affect the maneuverability and the safety of the aircraft. Because of this hazard, investigation into the onset and physics of buffet remains an important research direction for aerodynamics and transonic flight.

Since the discovery of transonic buffet, significant research has been devoted to investigating the phenomenon. Lee [2] provided a comprehensive review of theoretical and experimental studies of buffet from 1950 to 2000. Deck [3] conducted a numerical study using a detached-eddy-simulation model to capture the underlying flow physics. Xing et al. [4] examined the effects of time and grid resolution on computational accuracy. Crouch et al. [5,6] employed a flowfield global stability theory to analyze and predict the onset of buffet. Kenway and Martins [7] introduced such techniques as a separation sensor predictor and the lift curve break method for predicting buffet onset.

Buffet control has also long been an area of active research. A notable example of a buffet control mechanism is the shock control bump (SCB), which enhances wing or airfoil buffet behavior through modification of the upper surface shape to manipulate the airflow near the shock wave. Bruce and Colliss [8] provided an overall review of SCB research. The advantages and limitations of SCB were examined; and the challenges to SCB performance, including its sensitivity to flow conditions, were identified.

In the present work, a hybrid simulation–surrogate optimization method for supercritical airfoil design is developed. The objective is to reduce the drag and buffet magnitude, as well as to improve on the performance of the benchmark airfoil: OAT15A. Figure 2 illustrates

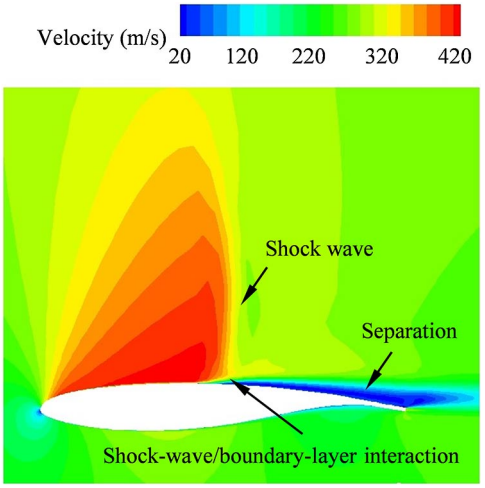

Fig. 1 Shock-wave/boundary-layer interaction for OAT15A airfoil at $M = 0.73$, and $\alpha = 3.5$ deg.

the overall process of airfoil design and optimization. First, a numerical scheme is implemented to detect and explore buffet behavior at the design flow condition ($M = 0.73$, $\alpha = 3.5$ deg). Results are then compared with existing experimental and computational data to verify the numerical scheme. Second, an airfoil shape modification method with 10 deg of freedom is developed to generate a set of new airfoils. We also introduce and impose a smoothness criterion on the new airfoils, which is generated in the form of a constraint on the second-order derivative of its geometry. This method eliminates the generation of "bumpy" airfoils before the numerical runs. Third, numerical simulations are performed for these new airfoils. Fourth, neural network (NN) surrogate models are established for mean aerodynamic coefficients and buffet parameters based on the numerical results of the new airfoils. Fifth, genetic algorithm (GA) optimization is conducted to identify the optimal airfoil profiles that minimize both the time-averaged drag coefficient $s^*_{\overline{c_d}}$, and the buffet magnitude s^*_A. To verify the accuracy of the optimal surrogate models, the behaviors of $s^*_{\overline{c_d}}$ and s^*_A at the design flow condition are simulated and compared with the values predicted by neural network modeling. Finally, the optimal airfoil profiles are compared with the benchmark airfoil: OAT15A. Their similarities and differences, in terms of their geometries, are discussed.

The remainder of this work is organized as follow. In Sec. II, we define the aerodynamics and buffet state variables for the NN modeling and optimization approach. In Sec. III, two optimization problems are stated, namely, drag reduction and minimization of buffet magnitude. In Sec. IV, the numerical scheme is introduced, and the computational method is verified through simulation of the OAT15A airfoil at $M = 0.73$, and $\alpha = 3.5$ deg. In Sec. V, the airfoil-profile perturbation method is introduced and a second-order smoothness criterion is used to generate a large set of new airfoils. In Sec. VI, NN modeling is used to build surrogate models for state variables. In Sec. VII, we use a GA to present the airfoil geometry optimization. In Sec. VIII, we analyze and discuss the optimal shapes (s^*_A and $s^*_{\overline{c_d}}$). Section IX presents the conclusions.

II. Buffet and Aerodynamics Parameters

In this section, we define metrics to measure the buffet and aerodynamics behaviors of the airfoil geometry. The time-averaged values of the lift and drag coefficients ($\overline{c_l}$, $\overline{c_d}$) are defined by Eqs. (1) and (2), respectively, to measure the aerodynamic behavior for an airfoil. The computational result presented in the following (Sec. IV) indicates the existence of transient and steadily oscillating buffet states; the steady oscillating state is the focus here. Leishman [9] proposed the concept of reduced frequency as a nondimensional frequency of aerodynamic or aeroelasticity phenomena. This concept is adopted for the dominant frequency in the lift coefficient spectral content. The relation between the dimensional frequency f and the reduced frequency k is shown in Eq. (3):

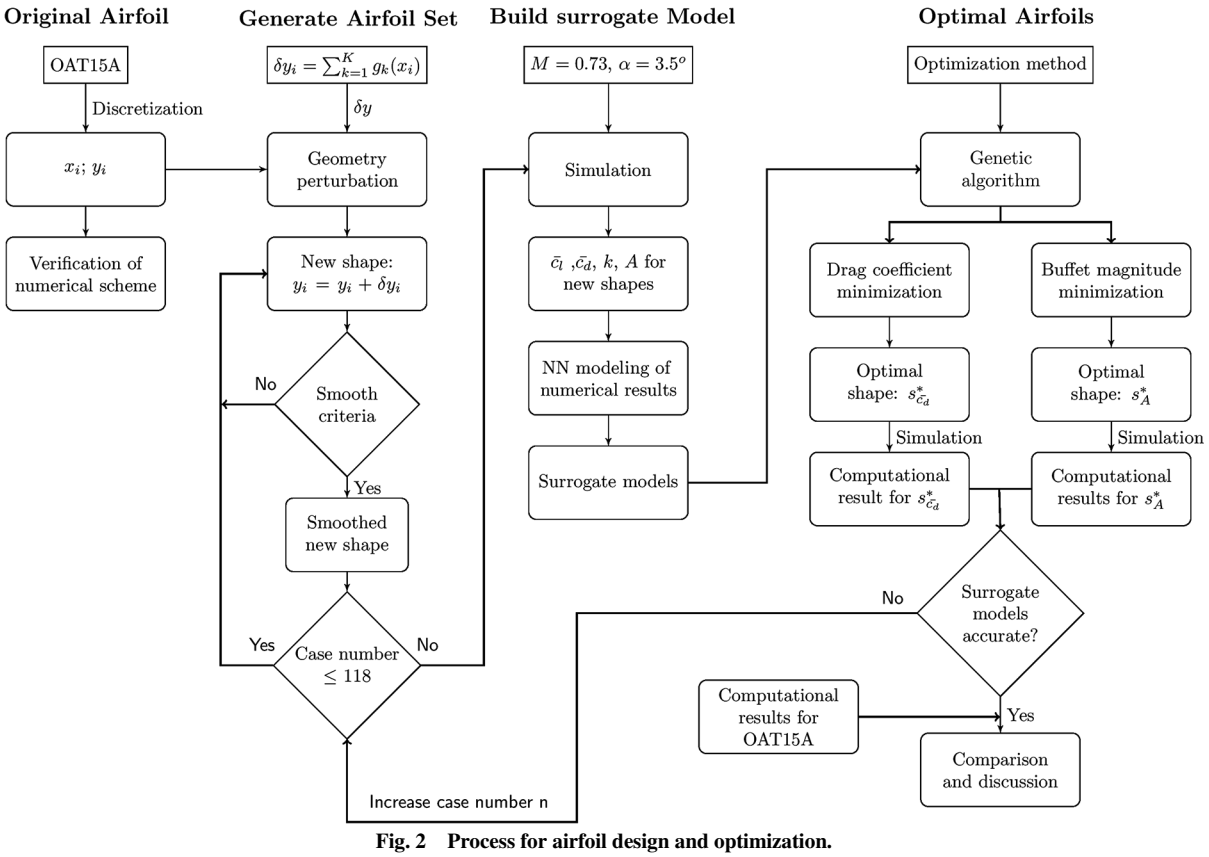

Fig. 2 Process for airfoil design and optimization.

$$\overline{c_l} = \frac{\Sigma c_{li}\delta t_i}{\Sigma \delta t_i} \tag{1}$$

$$\overline{c_d} = \frac{\Sigma c \delta t_i}{\Sigma \delta t_i} \tag{2}$$

$$k \triangleq \left(\frac{\pi \times c}{V_\infty}\right) \times f \tag{3}$$

The buffet magnitude A is defined as the amplitude of the aerodynamic force oscillation. From the computational results in Sec. VI, because the time-averaged lift coefficient is more than 10 times the mean drag coefficient for the OAT15A airfoil at the design flow condition, we will ignore the contribution of the drag component to the total force oscillation. The buffet magnitude is then characterized using the amplitude of the c_l oscillation in a steady oscillating state, as shown in Eq. (4):

$$A = \Delta c_{l\max} \tag{4}$$

III. Problem Statement

The major task in airfoil design and optimization is to reduce the drag coefficient while producing a required amount of lift. Furthermore, if the buffet phenomenon is considered, the magnitude of the buffet should be reduced and the oscillation frequency constrained. Airfoil optimization should therefore 1) reduce the time-averaged drag coefficient $\overline{c_d}$, and 2) reduce the buffet magnitude A. Note that k, A, $\overline{c_l}$, and $\overline{c_d}$ are set as state variables. The design variables are airfoil shape parameters (G_i), which will be discussed in Sec. V. The optimization problem is stated in Eqs. (5) and (6). To ensure that the optimal shapes will be superior to the benchmark airfoil in all aspects, we use state variables of the OAT15A airfoil ($\overline{c_{l\mathrm{OAT}}}$, $\overline{c_{d\mathrm{OAT}}}$, A_{OAT}, k_{OAT}), and we employ relaxation coefficients ($\zeta_{\overline{c_l}}$, $\zeta_{\overline{c_d}}$, ζ_A, ζ_k) to form the inequality constraints of the optimization problem. A genetic algorithm is applied to search for a global optimal design in Sec. VII.

Problem statement 1:

$$\begin{aligned} \text{minimize} \quad & \overline{c_d}(G_i) \\ \text{with regard to} \quad & G_i \\ \text{subject to} \quad & \overline{c_l} \geq (1+\zeta_{\overline{c_l}})\overline{c_{l\mathrm{OAT}}} \\ & 0 \leq A \leq (1-\zeta_A)A_{\mathrm{OAT}} \\ & 0 \leq k \leq (1-\zeta_k)k_{\mathrm{OAT}} \end{aligned} \tag{5}$$

Problem statement 2:

$$\begin{aligned} \text{minimize} \quad & A(G_i) \\ \text{with regard to} \quad & G_i \\ \text{subject to} \quad & \overline{c_l} \geq (1+\zeta_{\overline{c_l}})\overline{c_{l\mathrm{OAT}}} \\ & 0 \leq \overline{c_d} \leq (1-\zeta_{\overline{c_d}})\overline{c_{d\mathrm{OAT}}} \\ & 0 \leq k \leq (1-\zeta_k)k_{\mathrm{OAT}} \end{aligned} \tag{6}$$

IV. Numerical Framework, Results, and Validation

In this section, a numerical scheme is implemented to explore the buffet and aerodynamics state parameters for the OAT15A airfoil. The results are then validated against experimental and computational data on the OAT15A airfoil to confirm the suitability of the scheme.

A. Numerical Scheme

Figure 3 illustrates the numerical grid, which is a structural C grid, with 26,404 grid nodes and 26,066 grid cells, as well as a boundary at ±75 chord lengths. Two-hundred nodes on the airfoil surface are employed to calculate the lift and drag coefficient. A 0.6%-thick trailing edge is made in the computational grid. Barakos and Drikakis [10] noted that the Spalart–Allmaras (SA) turbulence model [11] could capture the buffet phenomenon, at a fair computational cost. The SA model is therefore used here, with the same constants as in Ref. [12]. The Sutherland viscous model [13] for ideal gas is used.

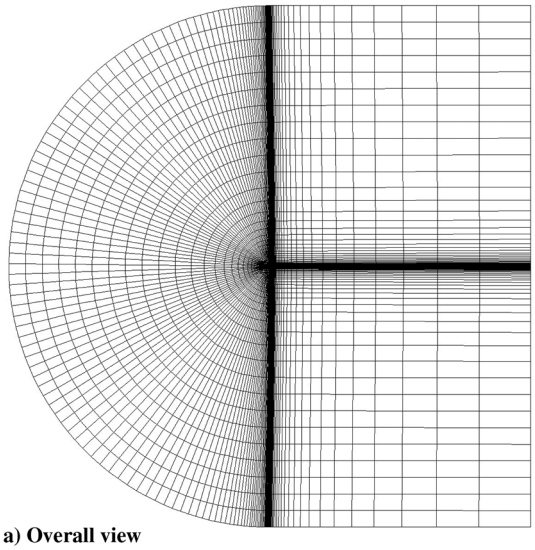

a) Overall view

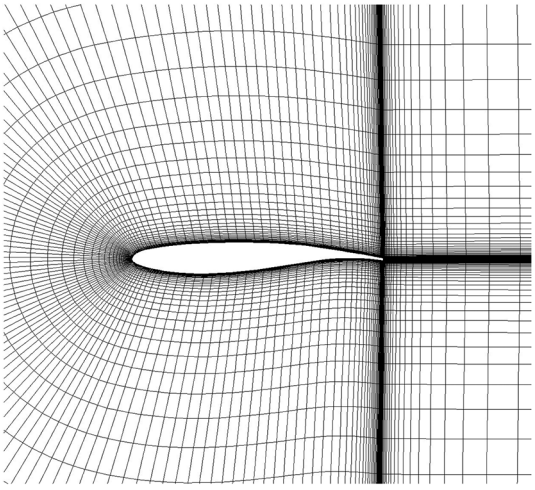

b) Near surface

Fig. 3 C-type computational grid for OAT15A airfoil.

Time-accurate calculations are required to capture the buffet phenomenon, and a fine time scheme is required. The physical time step δt is nondimensionalized to Δt as in Eq. (7). The dimensionless chord length is $c = 1$. The mean value and fluctuation parameters of c_l are considered, with different time steps, at the design flow condition. The computation is performed by means of the least-square cell-based gradient method with second-order upwind spatial discretization using Fluent software on a 2.5 GHz dual processor and 2.4 GB system memory machine. Numerical results are given in Table 1. Figure 4 shows the computational wall time T with different time-step sizes Δt.

Table 1 Calculated time-averaged lift coefficient and buffet behaviors with different numerical time steps Δt

Δt	$\overline{c_l}$	A	f
0.10	1.038	0	0
0.08	1.039	0	0
0.06	1.039	0.0036	69 Hz
0.04	1.041	0.0163	69 Hz
0.02	1.036	0.0316	69 Hz
0.01	1.037	0.0783	69 Hz
0.002	1.037	0.0796	69 Hz

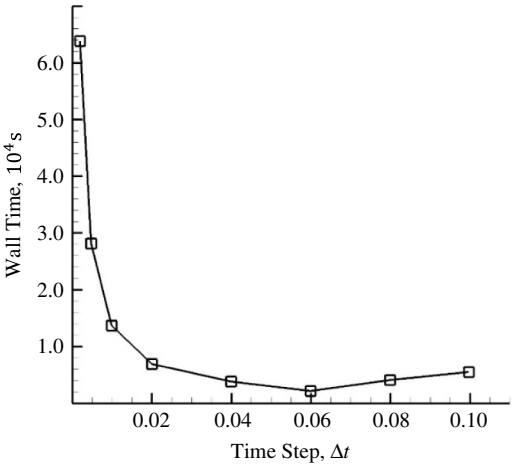

Fig. 4 Computational wall time with different numerical time steps Δt for numerical simulation of OAT15A airfoil.

The numerical scheme was not able to capture the buffet phenomenon for nondimensional time steps of $\Delta t \geq 0.08$, although it was resolved computationally for $\Delta t \leq 0.06$. However, although $\overline{c_l}$ and f appeared insensitive to Δt, the buffet amplitude A exhibited significant variations between $\Delta t = 0.02$ and 0.06. It leveled off for $\Delta t \leq 0.01$. The computational wall time decreased dramatically with Δt for $\Delta t \leq 0.02$, and it reached a minimum at $\Delta t = 0.06$. It varied slightly for $0.02 \leq \Delta \leq 0.10$.:

$$\Delta t = \delta t \times \frac{a_\infty}{c} \tag{7}$$

As a tradeoff between the numerical accuracy and efficiency, therefore, a nondimensional time step of $\Delta t = 0.01$, corresponding to the physical step of $\delta t = 2.94 \times 10^{-5}$ s, was chosen for the present computations. This choice allowed for accurate capturing of the different parameters of the buffet phenomenon at a reasonable computational cost.

Because the new airfoils generated here are based on small perturbations around the geometry of the benchmark airfoil (OAT15A), the same computational scheme and parameters are applied to these new airfoils.

B. Numerical Result for OAT15A Airfoil

The aerodynamic behaviors of the benchmark OAT15A airfoil at design flow condition are examined to assess the validity of the numerical scheme. Figure 5 shows the time histories of the lift and drag coefficient. They both oscillate periodically, with the magnitude growing to limit-cycle values at a dimensional time of $t \approx 0.12$ s. Given that $\delta t \approx 3 \times 10^{-5}$ s in the present study, 5000 time steps with a real-time interval of 0.15 s are enough to reach a steady oscillation state. The entire calculation runs for 11,000 steps, or 10 buffet periods. This allows for the collection of a statistically meaningful dataset. The FFT analysis for c_l and c_d are shown in Fig. 6.

The calculated $\overline{c_l}$, A, and f in the steady oscillating state are compared with both experimental [14] and computational [4] results for the OAT15A airfoil at the same flow condition in Table 2. The relative errors for the measured frequency are less than 1.5%, which are much better than the prediction of an existing study [4].

V. Airfoil Shape Modification and New Airfoil Generation

In this section, we develop an airfoil geometry modification method with a smoothness criterion, and we generate a new set of airfoils for the sample space of surrogate modeling. To modify the profile and populate the design space with new airfoils, the upper and lower surfaces of the OAT15A airfoil are discretized by $\Delta x = 0.008$ along the chord length direction. In Ref. [15], Drela suggested a set of trigonometric functions [Eqs. (8) and (9)] to modify the airfoil shape,

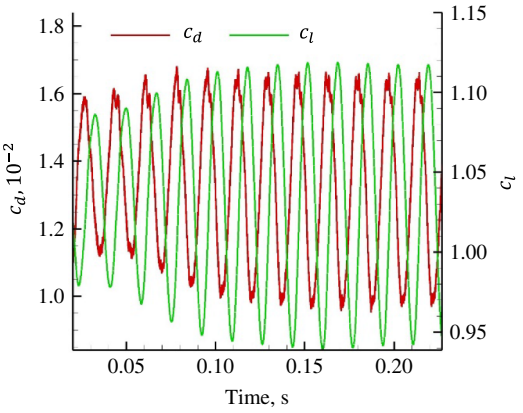

Fig. 5 Time evolution of lift and drag coefficients of OAT15A airfoil at the design flow condition.

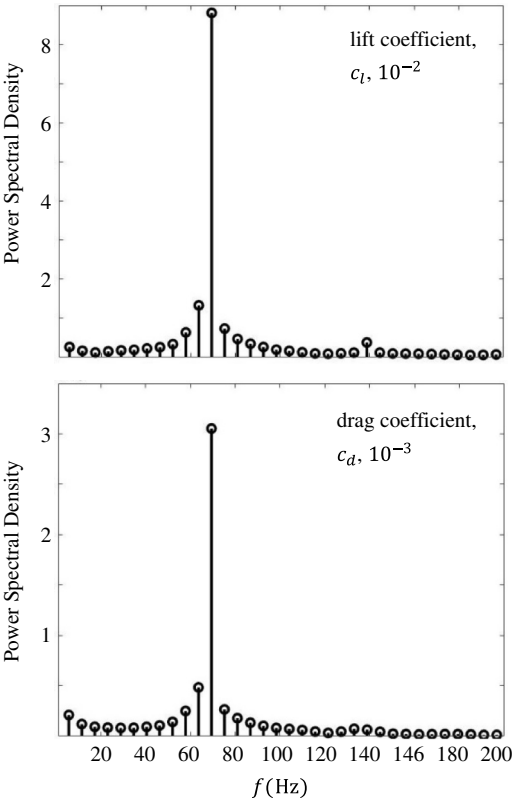

Fig. 6 Power spectral density of calculated lift and drag coefficients.

where $g_k(x)$ was a basic function with mode number k, G_k was a design parameter, and $D = 0.01$ was the amplitude of disturbance. Here, five modes are used for both the upper and lower surfaces. The design space has 10 deg of freedom:

$$g_k(x) = \frac{1}{k}\sin(k\pi x) \tag{8}$$

Table 2 Computational and experimental results for time-averaged lift coefficient, buffet magnitude, and frequency[a]

	$\overline{c_l}$	A	f
Present study	1.037	0.0881	69 Hz
Numerical result [4]	1.015	0.075	77 Hz
Experimental result [14]	N/A	N/A	70 Hz
Relative error vs reference numerical data	1.2%	14.8%	10.3%
Relative error vs experiment results	N/A	N/A	1.4%

[a]N/A denotes "not applicable."

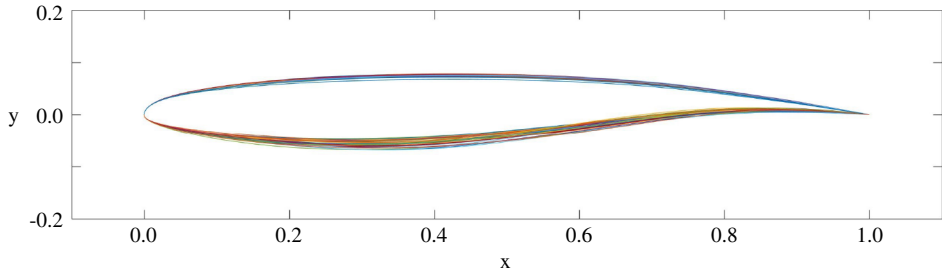

Fig. 7 New airfoil profiles generated with smoothness criteria.

Table 3 Boundaries for design variables of generated airfoils

Variable	G_1	G_2	G_3	G_4	G_5	G_6	G_7	G_9	G_{10}
Minimum	0.43	−0.35	−0.14	−0.18	−0.13	−1	−1	−0.57	−0.42
Maximum	1.0	0.54	0.47	0.21	0.23	1	0.5	1	0.69

$$\delta y = D \sum_{k=1}^{K} G_k g_k(x) \tag{9}$$

Although this set of basic functions guarantees the orthogonality for the design space, it results in bumpy shapes for the airfoil surface. Drela [15] noted that the bumpy shape could increase airfoil drag in offdesign flow conditions and contribute to stall. The following criteria are used to eliminate inferior profiles before numerical simulation of the new airfoils:

Criteria 1: The sign of d^2y/dx^2 changes once on the upper surface

Criteria 2: The sign of d^2y/dx^2 changes twice on the lower surface.

Because bumpiness is reflected in a sign change of the second-order derivative on the airfoil surface, these criteria eliminate the issue. Furthermore, the second criterion can maintain an aft camber for the lower surface, which is a key element in supercritical airfoil design to obtain lift without strong shocks [16]. To implement these criteria computationally, the second-order derivative is calculated by a forward and a backward finite difference method at the leading and trailing points, respectively, and a central difference scheme is used for interior nodes. Using this shape perturbation method and smoothness criteria, a new set of airfoils with random G_1 to G_{10} from −1 to 1 is generated. Considering the computational cost, we produce 118 geometries for the set of new airfoils, as shown in Fig. 7. The boundaries of the design variables are given in Table 3.

Table 4 Ranges of $\overline{c_l}$, $\overline{c_d}$, A and k

	$\overline{c_l}$	$\overline{c_d}$	A	k
Minimum	0.904	0.0082	0.0418	0.776
Maximum	1.074	0.0190	0.1720	1.063
Mean	0.994	0.0145	0.0834	0.929

Calculations were conducted for all 118 airfoil profiles. Figure 8 shows the histograms of the calculated state variables in the sample space. These ranges are given in Table 4. As expected, the time-averaged drag coefficient $\overline{c_d}$ and buffet magnitude A values are sensitive to airfoil geometry.

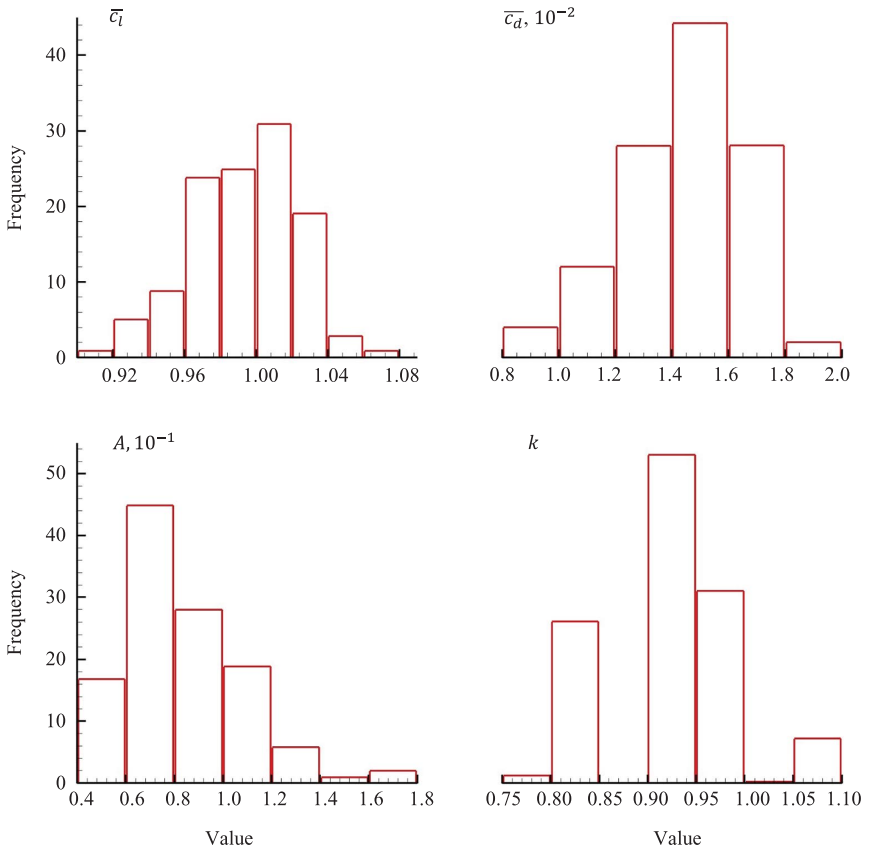

Fig. 8 Distribution of calculated aerodynamic and buffet parameters of 118 new airfoils.

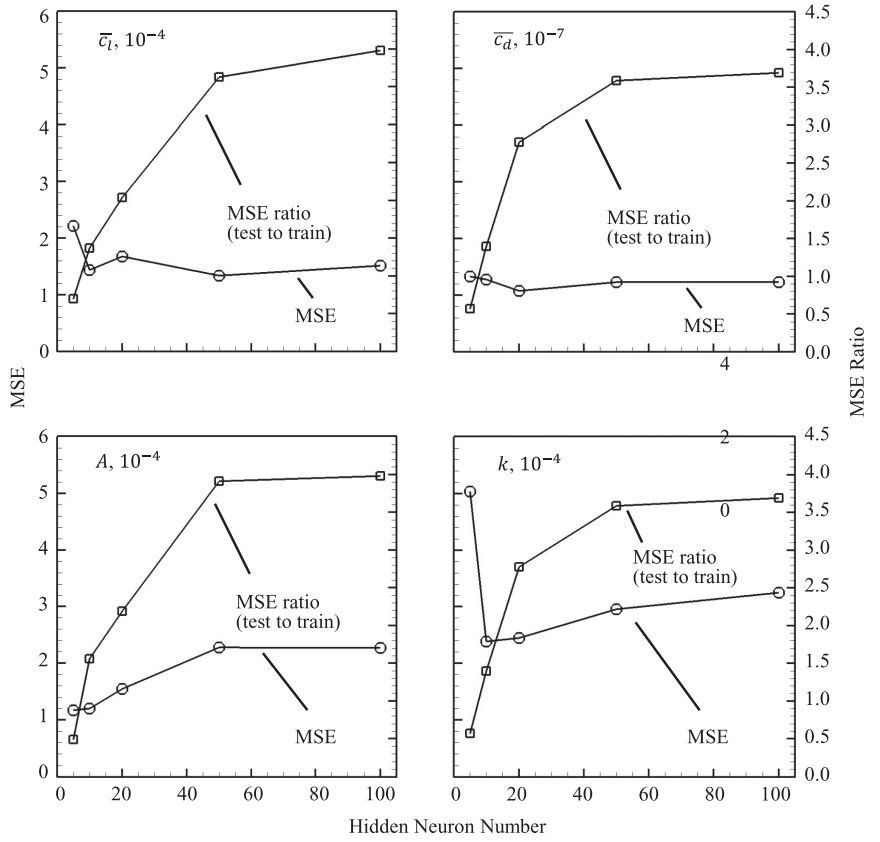

Fig. 9 Ratio of testing to training MSE and total MSE for 118 new shapes: trend with hidden neuron number.

VI. Neural-Network-Based Surrogate Models

In this section, surrogate models are constructed for new airfoils based on the numerical results using a neural network fitting method. The mean square error (MSE) and R^2 are used to assess the quality and effectiveness of the surrogate models. The MATLAB Neural Network Toolbox is employed to construct the fully connected network model based on the Levenberg–Marquardt backpropagation method [17]. The structure is a feedforward neural network with one hidden layer. In the construction of the neural network, 80% of the 118 numerical cases are randomly selected as training data, and 20% are used for testing and validation. The neuron numbers are chosen by the tradeoff between optimal fitting and computational cost. Although a model with more hidden neurons improves the fitting of the training data, overfitting happens for a large number of hidden neurons. Figure 9 shows the ratio of the MSE between the testing and training datasets, and the overall MSE for the 118 new airfoil shapes as a function of neuron numbers. The model performance is approximately constant or declines from 10 hidden neurons, and the MSE ratio increases dramatically. Meanwhile, a complex model with unnecessary neurons increases the computational workload for optimization. The Gnana and Deepa criteria [18] are applied for neuron number selection. Given the size of the input and output variables, 5–10 neurons are tested in the hidden layer, as shown in Fig. 10. Based on the MSE value, models with five hidden neurons for $\overline{c_d}$ and A, seven for k, and nine for $\overline{c_l}$ are used. Figures 11 and 12 show the histograms and normal probabilities of the surrogate model residuals for the aerodynamic and buffet parameters, respectively. The residuals lie on an approximately Gaussian distribution with a mean of zero. The MSE and R^2 of the models are given in Table 5. The quality of the neural network surrogate is compared with the second-order polynomial backward elimination stepwise regression method and the Gaussian process kriging method through the MSE and R^2 value (see the Appendix).

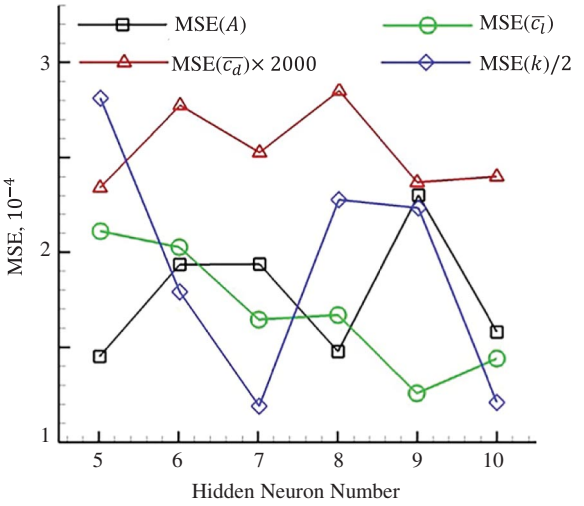

Fig. 10 MSE of state variables for different neural network surrogate topologies.

VII. Genetic Algorithm Global Optimization

The two constrained optimization problem statements for $\overline{c_d}$ and A are provided by Eqs. (5) and (6). A GA [19] is applied in this section to obtain the optimal airfoil design for each problem. It is a global optimizer, and it suffers drawbacks associated with its computational

Table 5 MSE and R^2 for NN-based surrogate models of 118 new airfoils

	$\overline{c_l}$	$\overline{c_d}$	A	k
MSE	1.26×10^{-4}	1.16×10^{-7}	1.45×10^{-4}	2.39×10^{-4}
R^2	0.865	0.974	0.791	0.914

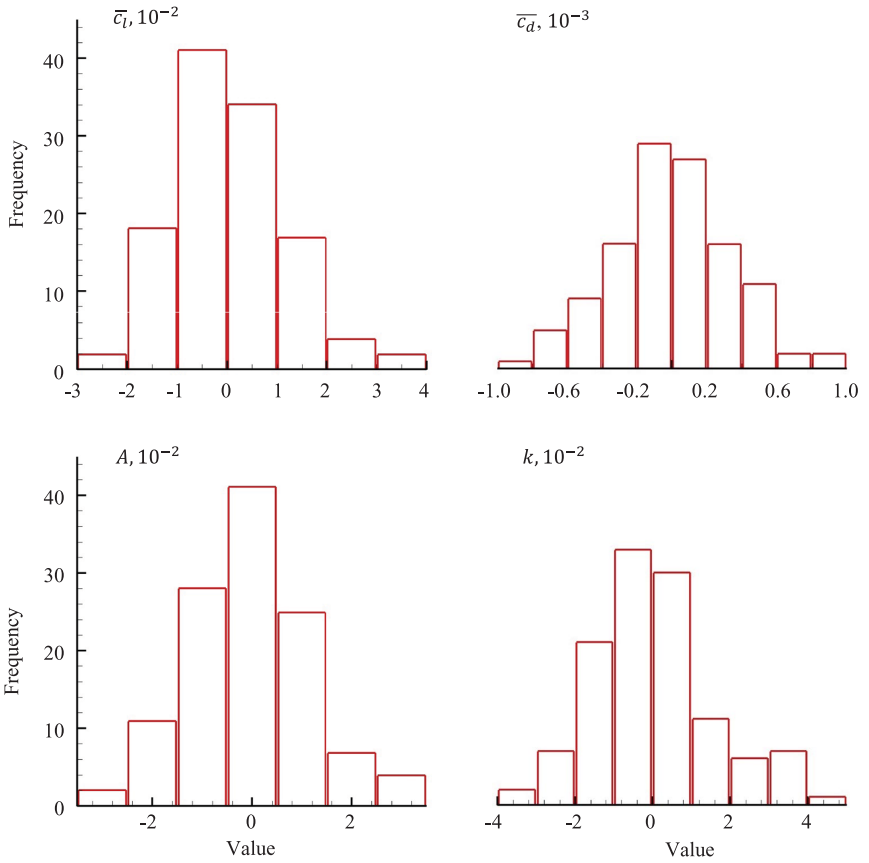

Fig. 11 Histograms of surrogate model residuals for aerodynamic and buffet parameters of 118 new airfoils.

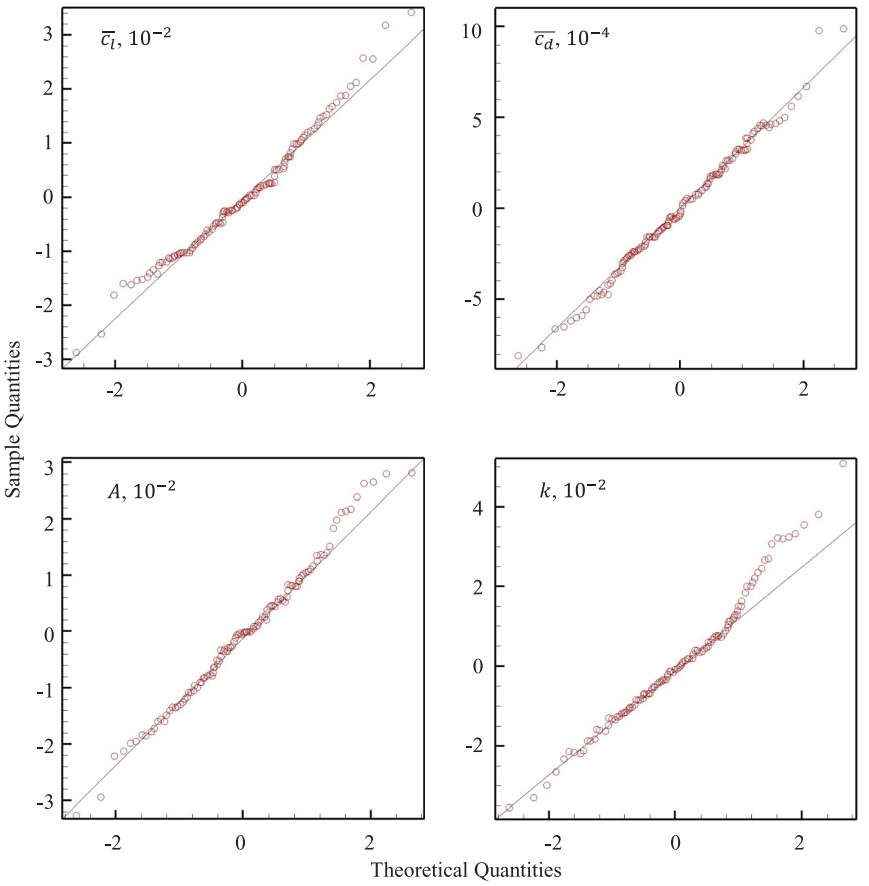

Fig. 12 Normal probabilities of surrogate model residuals for aerodynamic and buffet parameters of 118 new airfoils.

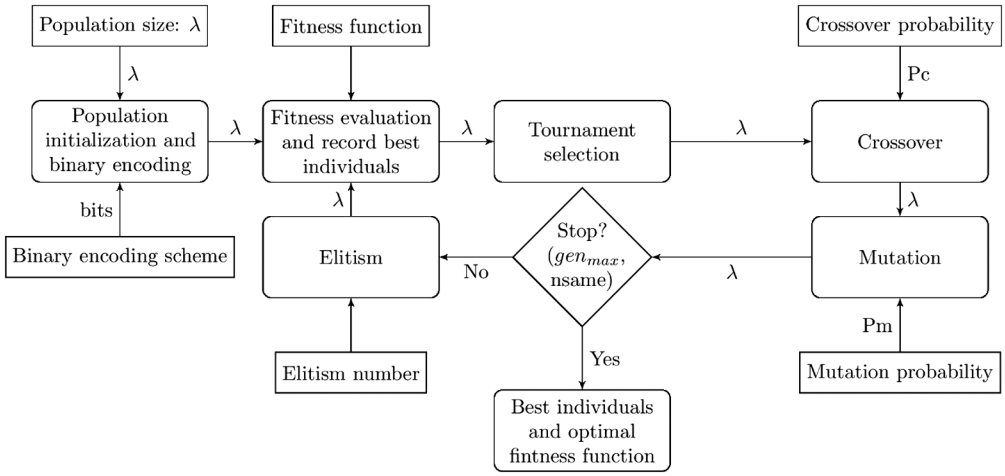

Fig. 13 Schematic of genetic algorithm optimization.

cost. For the two problems of concern, the parameters must be carefully selected to retain accuracy and reduce computational expense. Figure 13 schematically shows the GA used in the present study. A 10-bit-length chromosome is used to provide a resolution of 0.001, a crossover probability of $P_c = 0.7$, and a mutation probability of $P_m = 0.01$. The initial population is generated randomly with $\lambda = 300$, and a single point crossover is applied. The maximum generation number is $\text{gen}_{\max} = 300$, and the GA stops after 50 continuous generations with the same optimal individual ($i$same $= 50$). The optimization constraints are added to the fitness function through the penalty function from Eqs. (10–12) with $r = 10{,}000$. The drag and buffet magnitude optimizations are conducted with different values of ζ_k, $\zeta_{\overline{c_l}}$, $\zeta_{\overline{c_d}}$, and ζ_A, as given in Tables 6 and 7.

Table 6 Optimization results of time-averaged drag coefficient with different relaxation coefficients

$\zeta_{\overline{c_l}}$	ζ_k	ζ_A	$\overline{c_l}$	$\overline{c_d}$	A	k
0.01	0	0.01	1.054	0.0105	0.070	0.865
0.01	0	0.1	1.054	0.0105	0.070	0.865
0.01	0	0.2	1.054	0.0105	0.070	0.865
0.01	0.08	0.01	1.047	0.0126	0.063	0.795
0.01	0.08	0.1	1.047	0.0126	0.063	0.795
0.01	0.08	0.2	1.047	0.0126	0.063	0.795
0.05	0	0.01	1.088	0.0111	0.043	0.865
0.05	0	0.1	1.088	0.0111	0.043	0.865
0.05	0	0.2	1.088	0.0111	0.043	0.865
0.05	0.08	0.01	1.089	0.0118	0.045	0.795
0.05	0.08	0.1	1.089	0.0118	0.045	0.795
0.05	0.08	0.2	1.089	0.0118	0.045	0.795

Table 7 Optimization results of buffet magnitude with different relaxation coefficients

$\zeta_{\overline{c_l}}$	ζ_k	$\zeta_{\overline{c_d}}$	$\overline{c_l}$	$\overline{c_d}$	A	k
0.01	0	0.01	1.051	0.0121	0.022	0.865
0.01	0	0.1	1.051	0.0121	0.022	0.865
0.01	0	0.2	1.047	0.0109	0.043	0.865
0.01	0.08	0.01	1.047	0.0116	0.033	0.795
0.01	0.08	0.1	1.047	0.0116	0.033	0.795
0.01	0.08	0.2	1.047	0.0108	0.046	0.795
0.05	0	0.01	1.089	0.0119	0.042	0.865
0.05	0	0.1	1.089	0.0119	0.042	0.865
0.05	0	0.2	1.089	0.0109	0.060	0.865
0.05	0.08	0.01	1.088	0.0123	0.049	0.795
0.05	0.08	0.1	1.088	0.0123	0.049	0.795
0.05	0.08	0.2	1.088	0.0109	0.067	0.795

1) Because k is a discrete value from the fast Fourier transform analysis, the NN model outputs the expectation of k. A low-frequency oscillation is preferred because it is less harmful to the structure. We select $\zeta_k = 0$ and 0.08, which correspond to $f = 69$ and 64 Hz, and $k = 0.865$ and 0.795.

2) The time-averaged lift coefficient $\overline{c_l}$ is a strong constraint on both optimization problems. If we set $\zeta_{\overline{c_l}} > 0.05$ and $\overline{c_l} > 1.089$, no feasible optimal solution is available. On the other hand, ζ_A is a loose constraint in drag optimization.

3) For the drag minimization with $\zeta_k = 0$, the $\zeta_{\overline{c_l}} = 0.05$ case reduces 38% of A, and it only raises 5% of $\overline{c_d}$ over the $\zeta_{\overline{c_l}} = 0.01$ case. Therefore, $\zeta_k = 0$, $\zeta_{\overline{c_l}} = 0.05$ is a good selection for relaxation parameters. For buffet magnitude optimization, because A increases rapidly with $\zeta_{\overline{c_d}}$, $\zeta_{\overline{c_l}} = 0.01$, $\zeta_{\overline{c_d}} = 0.01$, and $\zeta_k = 0$ are reasonable choices:

$$p_i = \max(0, [i - (1 - \zeta_i) i_{\text{OAT}}])(i = \overline{c_l}, \overline{c_d}, k, A) \tag{10}$$

$$f_{c_d} = \overline{c_d} + r \times (p_{\overline{c_l}} + 10 p_A + p_k) \tag{11}$$

$$f_A = A + r \times (p_{\overline{c_l}} + 10 p_{\overline{c_d}} + p_k) \tag{12}$$

VIII. Results and Discussion

This section first presents the optimization results based on the surrogate models. These NN-optimized airfoil models are tested and verified with numerical simulations, and then the two optimal airfoil shapes are discussed: the time-averaged drag coefficient optimal shape $s^*_{\overline{c_d}}$, and the buffet magnitude optimal shape s^*_A. Suggestions for supercritical airfoil design are also offered.

A. Optimization Results

Table 8 shows the results for the design parameters (G_1–G_{10}) of the surrogate-based optimal airfoils.

B. Numerical Results for Optimal Airfoils

Once the surrogate-based optimal airfoils are obtained, they are examined using the calculated time-averaged drag coefficient $\overline{c_d}$ and buffet magnitude A at $Ma = 0.73$ and $\alpha = 3.5°$. Tables 9 and 10

Table 8 Design parameters for optimal airfoils $s^*_{\overline{c_d}}$ and s^*_A

Parameters	G_1	G_2	G_3	G_4	G_5	G_6	G_7	G_8	G_9	G_{10}
$s^*_{\overline{c_d}}$	0.430	0.316	0.459	−0.176	0.227	0.297	−0.835	0.991	−0.346	−0.099
s^*_A	0.471	0.156	4.418	−0.164	0.123	0.845	−0.614	0.921	−0.096	−0.186

Table 9 Aerodynamic and buffet parameters for the airfoil with the optimized time-averaged drag coefficient $s^*_{\overline{c_d}}$

	$\overline{c_l}$	$\overline{c_d}$	A	k
Surrogate model	1.047	0.0126	0.063	0.865
Numerical	1.039	0.0115	0.059	0.865
Residual	+0.008	+0.0011	−0.004	0
Relative error, %	0.76	8.6	6.3	0

Table 10 Aerodynamic and buffet parameters for the airfoil with optimized buffet magnitude s^*_A

	$\overline{c_l}$	$\overline{c_d}$	A	k
Surrogate model	1.051	0.0121	0.022	0.865
Numerical	1.041	0.0118	0.020	0.865
Residual	+0.01	+0.0003	+0.002	0
Relative error, %	1.0	2.4	9.1	0

Table 11 Calculated aerodynamic and buffet parameters for the OAT15A and optimized drag and buffet magnitude airfoils

	$\overline{c_l}$	$\overline{c_d}$	A	k	$\overline{c_l}/\overline{c_d}$
OAT15A	1.037	0.0137	0.0881	0.865	76
$s^*_{\overline{c_d}}$	1.039	0.0115	0.069	0.865	90
s^*_A	1.041	0.0118	0.020	0.865	88

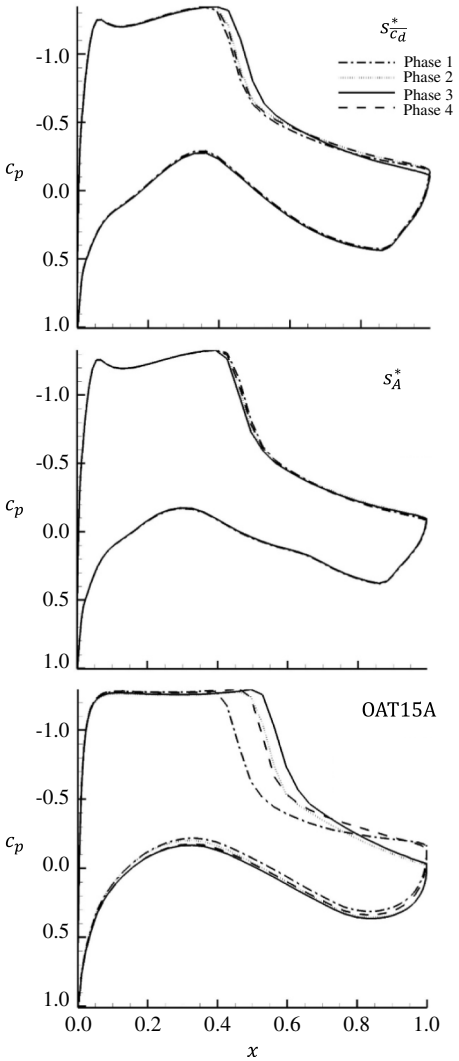

Fig. 14 Pressure distribution on OAT15A and optimized airfoils in different buffet phases.

compare the computational results with the surrogate model predictions.

Several observations can be made, based on the comparison between the NN-based surrogate model results and numerical simulations. First, good agreement between the two is achieved, with less than 10% relative error. Second, for the time-averaged lift coefficient and reduced frequency, the results are in excellent agreement for both optimal airfoils (less than 1% relative error). Finally, with regard to the discrepancies for the time-averaged drag coefficient and buffet magnitude, the surrogate model overestimates the two parameters by 6.3 and 9.1%, respectively, thereby providing conservative outcomes. These observations are interpreted to mean that the NN surrogate models provide valid approximations of the state parameters for the small disturbance design space of the airfoils generated. Improvements in the accuracy of the surrogate models for the time-averaged drag and buffet magnitude are left as a fruitful avenue for future work.

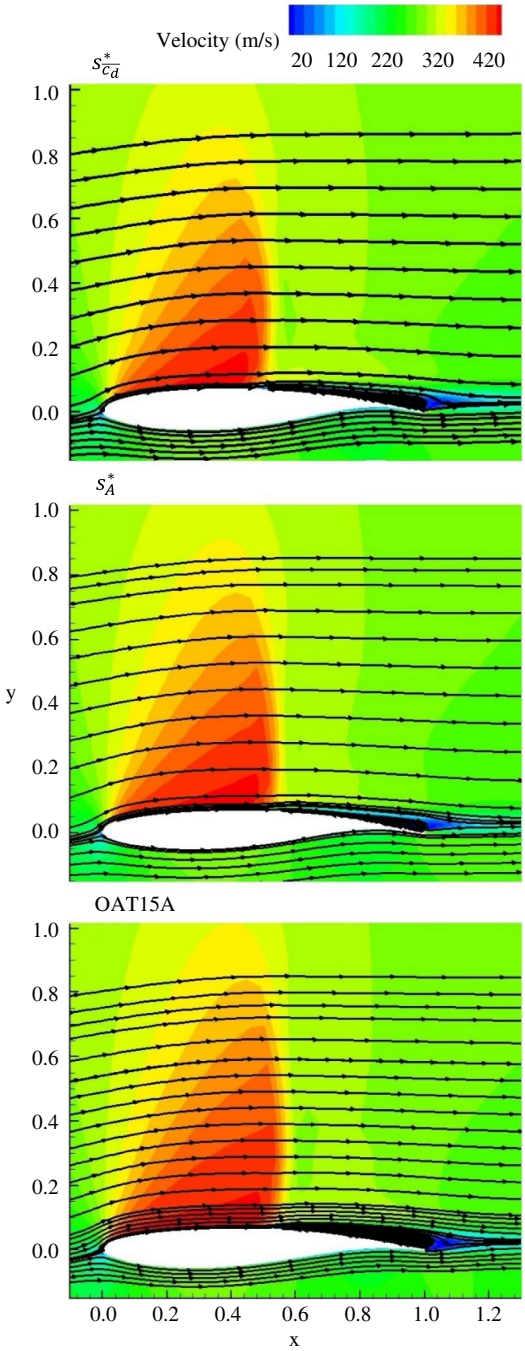

Fig. 15 Near-field velocity magnitude contours of OAT15A and optimized airfoils.

C. Optimal Airfoils Based on Drag and Buffet Magnitude

The two optimal airfoils, $s^*_{\overline{c_d}}$ and s^*_A, based on the minimized time-averaged drag coefficient and buffet magnitude are compared with the benchmark OAT15A airfoil. Table 11 shows the comparison result.

Although the time-averaged lift coefficients and reduced frequencies of airfoils are virtually identical, the optimal airfoils offer some improvement over the benchmark OAT15A airfoil in terms of the time-averaged drag coefficient. In addition, both optimal airfoils provide significant reduction of buffet magnitude over the OAT15A airfoil. For example, our s^*_A provides an impressive 70% reduction of buffet magnitude as compared with the OAT15A airfoil.

Both of the optimal airfoils achieve this buffet magnitude reduction by restricting the wave oscillation region. Figure 14 shows shock oscillation from roughly 0.4 to 0.45c for $s^*_{\overline{c_d}}$, and from 0.4 to 0.41c for s^*_A; both are significantly smaller than the range of 0.4–0.6c on the OAT15A airfoil. The buffet phases in Fig. 14 follow the oscillation cycle definition in Ref. [4]: the shock starts at the leading edge (phase 1) and moves to the trailing point (phase 3). Phases 2 and 4 are middle points of phase 1 and phase 3. Figure 15 shows the near-field velocity magnitude contour for OAT15A and two optimal shapes. It shows that the magnitude of the shock wave and separation zone is considerably reduced in the optimized shapes over the benchmark design. The drag for the optimal airfoils is decreased from the reduction of the intensity of the shock wave and separation zone. Meanwhile, the reduction of the shock and separation zone intensity reduces the unsteadiness of the flowfield, and the buffet amplitude is reduced.

Figure 16 overlays the geometries of the three airfoils: $s^*_{\overline{c_d}}$, s^*_A, and OAT15A. It is clear that the optimal shapes have a flatter upper surface than the OAT15A airfoil. Such a flat surface is important for supercritical airfoil design because it can weaken the shock and decrease the oscillation amplitude [16]. Furthermore, our optimal airfoils have a thinner trailing edge than the OAT15A airfoil. Physically speaking, a thinner trailing edge creates a smaller disturbance for the flowfield, thereby preventing the formation of pressure divergence, which is a major source of profile drag. In addition, the thin trailing edge can reduce the pressure wave produced by the trailing edge. Lee [2] described the impact of the upstream propagation of the pressure wave and feedback mechanism for buffet onset and the self-sustained wave oscillation. This modification can thus effectively reduce the buffet oscillation and its magnitude.

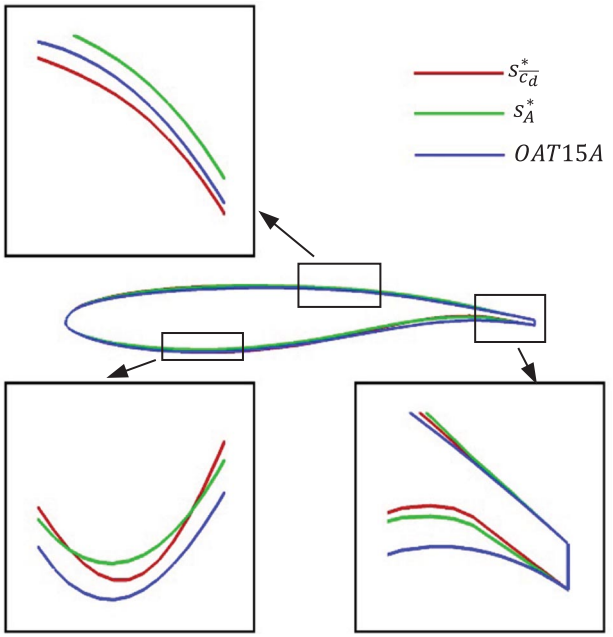

Fig. 16 Geometries of buffet-optimal airfoil, drag-optimal airfoil, and OAT15A airfoil.

IX. Conclusions

The present work describes a configuration optimization for a supercritical airfoil with a transonic buffet effect. As a characteristic transonic aerodynamics problem, buffet is caused by shock-wave/boundary-layer interaction, and it has a strong influence on transonic aviation. Although a full understanding of this nonlinear and complicated fluid mechanics phenomenon is not yet available, it is necessary to consider buffet effect in airfoil design. The objective of the present study is to establish a hybrid optimization-/neural-network-based surrogate modeling technique to optimize airfoils in terms of time-averaged drag and buffet magnitude. First, a numerical scheme is implemented to capture the buffet phenomenon. Then, an airfoil shape modification method with 10 deg of freedom and a second-order derivative smoothness criterion is developed. A total of 118 new airfoils are generated and simulated as the sample space for surrogate modeling. Then, surrogate models are developed to estimate airfoil behaviors. Next, a constrained optimization process is applied to determine optimal profiles. Finally, the optimal shapes are numerically analyzed, based on their computational results and their geometry.

Some of the key findings in the present work are as follows:

1) A fine time resolution is required in numerical simulations to accurately capture buffet magnitude.

2) A neural-network model is appropriate to model unsteady nonlinear aerodynamic phenomena such as transonic buffet.

3) The time-averaged drag coefficient $\overline{c_d}$ and buffet magnitude A are sensitive to airfoil geometry, and it is possible to reduce them simultaneously by configuration optimization.

4) The optimization process based on these surrogate models, which would have been impossible with a full numerical analysis with a genetic algorithm, is both computationally efficient and meaningfully accurate.

5) The resultant optimal airfoils, with a flatter upper surface and thinner trailing edge, provide meaningful improvements over the OAT15A in terms of the reduction of the mean drag coefficient and buffet magnitude, with the latter being the more hazardous concern.

It can be argued that there is a credible physical basis for these computationally obtained features and, indeed, that they contribute to meaningfully reducing buffet oscillation and its magnitude.

This work raises a series of important questions for future work. First, it is proposed to examine the relation between uncertainty quantification in the surrogate models and the initial set of airfoils used in the numerical analysis (here, 118). For example, although the current surrogate models for the time-averaged drag coefficient and the reduced frequency are fairly accurate ($R^2 = 0.974$ and 0.914, respectively), their accuracy for the time-averaged lift coefficient and buffet magnitude, although adequate, can be improved ($R^2 = 0.865$ and 0.791, respectively). This is probably achievable by increasing the number of initial numerical runs for a larger number of airfoils. Second, this work is carried out at a specific design flow condition ($M = 0.73$, $\alpha = 3.5$ deg) for which prior experimental and computational results are available for the OAT15A airfoil. This restriction is, in a sense, necessary to crosscheck and validate the method. Future work should examine the robustness of the current optimal airfoils under a broader range of design flow conditions. The objective is to identify and compare the buffet behavior envelope for different airfoils across a range of flight conditions. Finally, if these two analyses confirm the current findings (namely, the ability to design supercritical airfoils with significantly improved buffet behavior across a range of flight conditions), the work can be transitioned to an experimental phase with wind-tunnel testing of the buffet-optimized airfoils.

Appendix: Neural Network, Kriging, and Regression Model Comparison

A comparison of the neural network surrogate, kriging, and second-order polynomials with the backward elimination stepwise regression method for 118 new airfoils is shown in Table A1.

Table A1 MSE and R^2 for NN surogate, kriging, and regression methods for 118 new airfoils

Method		Neural network	Kriging	Regression
MSE	$\overline{c_d}$	1.16×10^{-7}	1.30×10^{-7}	1.20×10^{-7}
	$\overline{c_l}$	1.26×10^{-4}	2.94×10^{-4}	1.86×10^{-3}
	k	2.39×10^{-4}	2.77×10^{-4}	6.33×10^{-4}
	A	1.45×10^{-4}	1.43×10^{-4}	1.71×10^{-4}
R^2	$\overline{c_d}$	0.974	0.970	0.973
	$\overline{c_l}$	0.865	0.686	0.801
	k	0.914	0.900	0.772
	A	0.791	0.793	0.753

Acknowledgment

This work was supported by the William R. T. Oakes Endowment of the Georgia Institute of Technology.

References

[1] Hilton, W., and Fowler, R., "Photographs of Shock Wave Movement," Ministry of Supply, Aeronautical Research Council R&M 692, London, Dec. 1947, http://naca.central.cranfield.ac.uk/reports/arc/rm/2692.pdf [retrieved 2018].

[2] Lee, B., "Self-Sustained Shock Oscillation on Airfoils at Transonic Speeds," *Progress in Aerospace Science*, Vol. 37, No. 2, 2001, pp. 147–196. doi:10.1016/S0376-0421(01)00003-3

[3] Deck, S., "Numerical Simulation of Transonic Buffet over a Supercritical Airfoil," *AIAA Journal*, Vol. 43, No. 7, 2005, pp. 1556–1566. doi:10.2514/1.9885

[4] Xing, Y., Wang, G., Liu, Y., and Mian, H. H., "Numerical Investigation of Shock Oscillation In Transonic Buffeting Flow," *12th Applied Science and Tech.*, IEEE, Islamabad, Pakistan, Jan. 2015, pp. 473–480. doi:10.1109/ibcast.2015.7058545

[5] Crouch, J. D., Garbaruk, A., Magidov, D., and Travin, A., "Origin of Transonic Buffet on Aerofoils," *Journal of Fluid Mechanics*, Vol. 628, 2009, pp. 357–369. doi:10.1017/S0022112009006673

[6] Crouch, J., Garbaruk, A., and Magidov, D., "Predicting the Onset of Flow Unsteadiness Based on Global Instability," *Journal of Computational Physics*, Vol. 224, No. 2, 2007, pp. 924–940. doi:10.1016/j.jcp.2006.10.035

[7] Kenway, G. K., and Martins, J., "Aerodynamic Shape Optimization of the CRM Configuration Including Buffet-Onset Conditions," AIAA Paper 2016-1249, 2016. doi:10.2514/6.2016-1294

[8] Bruce, P., and Colliss, S., "Review of Research on Shock Control Bumps," *Shock Waves*, Vol. 25, No. 5, 2015, pp. 451–471. doi:10.1007/s00193-014-0533-4

[9] Leishman, J. G., *Principles of Helicopter Aerodynamics*, Cambridge Univ. Press, Cambridge, England, U.K., 2002.

[10] Barakos, G., and Drikakis, D., "Numerical Simulation of Transonic Buffet Flows Using Various Turbulence Closures," *International Journal of Heat and Fluid Flow*, Vol. 21, No. 5, 2000, pp. 620–626. doi:10.1016/S0142-727X(00)00053-9

[11] Spalart, P., and Allmaras, S., "A One-Equation Turbulence Model for Aerodynamic Flows," *La Recherche Aérospatiale*, Vol. 5, No. 1, 1994, pp. 5–21; also *30th Aerospace Sciences Meeting and Exhibit, Aerospace Sciences Meetings*, AIAA Paper 1992-0439, 1992. doi:10.2514/6.1992-439

[12] "Turbulence Modeling Resource: The Spalart—Allmaras Turbulence Model" (online database), NASA Langley Research Center, Hampton, VA, https://turbmodels.larc.nasa.gov/spalart.html [retrieved 06 June 2018].

[13] Sutherland, W., "The Viscosity of Gases and Molecular Force," *London, Edinburgh, and Dublin Philosophical Magazine and Journal of Science*, Philosophical Magazine Series 5, Vol. 36, No. 223, 1893, pp. 507–531. doi:10.1080/14786449308620508

[14] Jacquin, L., Molton, P., Deck, S., Maury, B., and Soulevant, D., "Experimental Study of Shock Oscillation over a Transonic Supercritical Profile," *AIAA Journal*, Vol. 47, No. 9, 2009, pp. 1985–1994. doi:10.2514/1.30190

[15] Drela, M., "Pros and Cons of Airfoil Optimization," *Frontiers of Computational Fluid Dynamics*, World Scientific, Singapore, 1998, pp. 363–381. doi:10.1142/9789812815774_0019

[16] Mason, W. H., "Transonic Aerodynamics of Airfoil and Wings Lecture Notes on Configuration Aerodynamics Class," Virginia Polytechnic Inst. and State Univ., March 2006, http://www.dept.aoe.vt.edu/~mason/Mason_f/ConfigAeroTransonics.pdf, [retrieved 10 March 2006].

[17] Yu, H., and Wilamowski, B., *Levenberg Marquardt Training, Industrial Electronics Handbook*, 2nd ed., Vol. 5, CRC Press, Boca Raton, FL, 2011, Chap. 12. doi:10.1201/noe1439802892

[18] Gnana, S., and Deepa, S., "Review on Methods to Fix Number of Hidden Neurons in Neural Networks," *Mathematical Problems in Engineering*, Vol. 2013, 2013, pp. 1–11. doi:10.1155/2013/425740

[19] Whitley, D., "A Genetic Algorithm Tutorial," *Statistics and Computing*, Vol. 4, No. 2, 1994, pp. 65–85. doi:10.1007/BF00175354

D. Harursampath
Associate Editor